

**Raman spectroscopy and X-ray diffraction responses when measuring health-related micrometre and nanometre particle size fractions of crystalline quartz and the measurement of quartz in dust samples from the cutting and polishing of natural and artificial stones**

STACEY, Peter, HALL, Samantha, STAGG, Stephen, CLEGG, Francis <<http://orcid.org/0000-0002-9566-5739>> and SAMMON, Chris <<http://orcid.org/0000-0003-1714-1726>>

Available from Sheffield Hallam University Research Archive (SHURA) at:

<http://shura.shu.ac.uk/28600/>

---

This document is the author deposited version. You are advised to consult the publisher's version if you wish to cite from it.

**Published version**

STACEY, Peter, HALL, Samantha, STAGG, Stephen, CLEGG, Francis and SAMMON, Chris (2021). Raman spectroscopy and X-ray diffraction responses when measuring health-related micrometre and nanometre particle size fractions of crystalline quartz and the measurement of quartz in dust samples from the cutting and polishing of natural and artificial stones. *Journal of Raman Spectroscopy*.


---

**Copyright and re-use policy**

See <http://shura.shu.ac.uk/information.html>

**RESEARCH ARTICLE**

# Raman spectroscopy and X-ray diffraction responses when measuring health-related micrometre and nanometre particle size fractions of crystalline quartz and the measurement of quartz in dust samples from the cutting and polishing of natural and artificial stones

Peter Stacey<sup>1,2</sup>  | Samantha Hall<sup>1</sup> | Stephen Stagg<sup>1</sup> | Francis Clegg<sup>2</sup> | Christopher Sammon<sup>2</sup>

<sup>1</sup>Buxton Laboratory, Health and Safety Executive, Buxton, UK

<sup>2</sup>Materials and Engineering Research Institute, Sheffield Hallam University, Sheffield, UK

**Correspondence**

Peter Stacey, Buxton Laboratory, Health and Safety Executive, Harpur Hill, Buxton, Derbyshire SK17 9JN, UK.  
Email: peter.stacey@hse.gov.uk

**Funding information**

Health and Safety Executive, Grant/Award Number: PH00760

**Abstract**

Around 560 000 workers in Great Britain are potentially exposed to respirable crystalline silica (RCS), which can cause disabling diseases, such as silicosis and lung cancer. These experiments assessed the performance of a new Raman spectroscopy method for measuring RCS, in samples of pure quartz powder with different median aerodynamic particle diameters and stone dusts from variety of natural and artificial stones. The relationship between the Raman response and particle size was characterised by measuring subfractions of the respirable quartz standard A9950 collected using the Sioutas impactor. Bulk samples of quartz standards A9950 and Quin B that provided the highest median particle size diameters were also measured. Health-related thoracic and respirable particle size fractions, and the environmental monitoring fractions of PM<sub>10</sub>, PM<sub>2.5</sub>, PM<sub>1</sub> and PM<sub>0.5</sub>, were also collected during the powered cutting and polishing of sandstone and diorite (granite), engineered and sintered stones. All Raman spectroscopy results were compared with those from X-ray diffraction (XRD), which was used as the reference technique. The Raman spectroscopy response closely followed the predicted crystallinity of RCS for different particle diameters. Raman spectroscopy obtained slightly higher percentages than XRD for particle size fractions below 1 µm. The Raman spectroscopy and XRD results were highly correlated for the thoracic, respirable and impactor fractions. The coefficients of determination were between 0.98 and 0.95. The slope coefficients for the correlation were 1.11 for the respirable fraction and 1.07 for the thoracic fraction. Raman spectroscopy is a promising alternative to XRD for measurement of RCS with a much lower limit of detection of 0.21 µg compared with 1 µg.

This is an open access article under the terms of the Creative Commons Attribution License, which permits use, distribution and reproduction in any medium, provided the original work is properly cited.

© 2021 Crown copyright. *Journal of Raman Spectroscopy* published by John Wiley & Sons Ltd. This article is published with the permission of the Controller of HMSO and the Queen's Printer for Scotland.

**KEYWORDS**

artificial stone, measurement, nanometre, particle size, respirable crystalline silica

**1 | INTRODUCTION**

This study was designed to support research to compare the particle size emission profile of aerosols generated from the powered cutting and polishing of natural and artificial stones. Industrial processes, using materials containing crystalline silica, can generate aerosols containing respirable (respirable crystalline silica [RCS]) particles that are small enough to penetrate to the alveoli region of the lung and can cause diseases like silicosis<sup>[1]</sup> and lung cancer.<sup>[2]</sup> It is estimated that 560 000 workers are regularly exposed to RCS in Great Britain<sup>[3]</sup> and 1.7 million in the United States.<sup>[4]</sup> One approach to assess exposure to hazardous airborne substances is to measure the concentration of the material entering the breathing zone of a worker. A sample of the aerosol is collected, using a sampler that selects sizes of particles that are associated with the main health effect. There are several different health-related size fractions that are of interest to researchers when evaluating the occupational health risk from aerosols of dust. The three size fractions that are of significance in occupational hygiene are for particle diameters that can penetrate into the nose and throat (inhalable), the larynx (thoracic) and the alveoli (respirable).<sup>[5]</sup> Respirable sized particles are associated with silicosis caused by inhalation of particles of crystalline silica. The respirable and thoracic fractions are subfractions of the inhalable dust that penetrate beyond the larynx and into the lung. The inhalable fraction contains particles that do not penetrate as far as the lung, where silicosis and lung cancer can occur, so this size fraction was not evaluated in this study. Differences between each particle size definition are shown in Figure S1.

The thoracic aerosol samplers are designed to select particles with a log-normal cumulative distribution of aerodynamic diameters that are less than 40  $\mu\text{m}$  and have a median of 10  $\mu\text{m}$ . Respirable samplers are designed to select particles with diameters of less than 16  $\mu\text{m}$  and a median diameter of 4  $\mu\text{m}$ . These particle size fractions differ from those used when measuring aerosol particulates in environmental atmospheres, which are termed PM10 for all particulate diameters less than 10  $\mu\text{m}$ , PM2.5 for particulate diameters less than 2.5  $\mu\text{m}$  and PM1 for particulate diameters less than 1  $\mu\text{m}$ . Aerosol samplers in environmental monitoring are designed to select the particle diameters with a more refined size selection cut within a specific standard deviation.<sup>[6]</sup> PM10 is comparable with the thoracic particle size health

fraction, and PM2.5 is used to specifically inform on the risks to health from those particles likely to penetrate to the gas exchange region (alveoli) of the lung.<sup>[7]</sup> Particle size fractions of PM2.5 and PM1 (particles equal to or less than 2.5 or 1  $\mu\text{m}$ ) are also of interest because these particles have greater potential to deposit in the alveoli.

X-ray diffraction (XRD) and Fourier transform infrared spectroscopy (FTIR) are two techniques that are currently employed for the measurement of concentrations of RCS in workplace aerosols.<sup>[8]</sup> Each technique employs a different principle of measurement. XRD measures the intensity of X-ray radiation diffracted from the arrangement of atoms within the structure of a crystalline component in the dust sample, whereas FTIR measures the absorbance of infrared radiation, which, for RCS, is related to the asymmetric Si–O–Si stretching and Si–O bending vibrations of the silicon and oxygen atoms in the crystalline silica.

Two significant factors that affect the accuracy of XRD and FTIR measurements of crystalline silica in dusts are the presence of interferences (i.e., other crystalline components with reflections or absorbance that coincides with those from crystalline silica) and the particle size and crystallinity of the measured material. The particle size of the RCS in a sample of dust affects the measurement response for both XRD and FTIR.<sup>[9]</sup> FTIR absorbance increases as the particle size decreases from about 8 to 1  $\mu\text{m}$  in diameter,<sup>[10,11]</sup> whereas XRD integrated area intensity measurements are more consistent over this particle size range.<sup>[9,12,13]</sup> The measurement response per unit mass of both FTIR<sup>[10]</sup> and XRD<sup>[9,12]</sup> shows an attenuation at particle diameters less than 1  $\mu\text{m}$ . The reduction in measurement response for both XRD and FTIR is attributed to a thin amorphous, or less ordered, layer on the surface of each crystalline silica particle of approximately 0.03  $\mu\text{m}$  in depth that transitions into a more crystalline centre.<sup>[10,14–16]</sup> The less crystalline surface layer contributes proportionately more, in terms of particle volume and mass, at particle diameters less than 1  $\mu\text{m}$ , so that both the XRD and FTIR techniques give lower measurement responses for the mass of crystalline silica particles. The mass of crystalline silica in the aerosol would be under-reported, if the reference material used for calibrating each instrument contained significant numbers of larger particles (equal or greater than 1  $\mu\text{m}$ ), than those in the collected aerosol.

Raman spectroscopy has been widely used for the characterisation of individual aerosol particles<sup>[17–20]</sup>;

however, it is a relatively new technique for the quantitative analysis of hazardous substances in aerosols collected for occupational hygiene exposure measurements.<sup>[20–23]</sup>

The aim of this work is to assess if particle size is a factor that affects the Raman band intensity when using the specific analytical conditions proposed for a new method to measure aerosols of RCS collected onto filters.<sup>[24]</sup> Another aim of this study is to compare results obtained using Raman spectroscopy, as a new method to measure RCS, with those obtained from the established technique of XRD for both laboratory generated samples and emissions collected during typical stone working activities.

Particle size can affect the measured Raman spectroscopy response, and micro-Raman spectroscopy is used as a technique to measure the particle size of nano-sized particles.<sup>[25]</sup> The profile and position of the Raman band can change as the particle diameter decreases.<sup>[26]</sup> The role of particle size and its effect on near infrared (NIR) Raman scattering in loose powders and tablets were described by Schrader et al.<sup>[27,28]</sup> Equation 1 was used to explain the scattering of the Raman band intensity emitted from the substance in an anti-parallel direction from a sample, that is, with a measurement arrangement that is similar to the modern Raman spectrometers with microscope attachments used in this work.

$$J_{Scattered} = \Phi \frac{sk}{\alpha} \frac{k \sinh kd + (\alpha + r) \sinh kd \cosh kd - krd}{[(\alpha + r) \sinh kd + k \cosh kd]^2} \quad (1)$$

where  $k^2 = 2r\alpha + \alpha^2$ ,  $\alpha$  is the absorption coefficient,  $r$  is the elastic scattering coefficient,  $s$  is the Napierian (internal) scattering coefficient,  $d$  is the depth of sample and  $\Phi$  is the applied flux. The elastic scattering coefficient ( $r$ ) is inversely proportional to the diameter of the particles,<sup>[28]</sup> which would imply that scattering would be greater in powders for larger diameter grains.

The principal theoretical findings of Schrader et al.<sup>[28]</sup> were that Raman intensity should

- increase as the particle size increases;
- increase when the depth of the sample increases, which reaches a stationary value at small sample thickness for fine powders; and
- be independent of the size of grains when measuring small particles with optimised conditions (i.e., in cuvettes with reflective surfaces).

However, the intensity ( $I$ ) of the Raman band response observed by the detector through the instrument is also dependent on a number of other factors (Equation 2), which includes the wavenumber of the energy source ( $\bar{\nu}_0$ ); the Raman shifted wavenumber ( $\Delta\bar{\nu}$ ); the reference wavenumber ( $\bar{\nu}_{ref}$ ); the applied power of the energy source ( $\Phi$ ); the cross-sectional area of the laser beam on the sample ( $A$ ); the depth of the sample ( $d$ ); the number of molecules per unit volume irradiated ( $N$ ); and the differential Raman photon scattering cross-section (the proportion of photons [ $J_{scattered}$ ] effectively scattered by the incident radiation) ( $\beta$ ):

$$I = \frac{\Phi}{A} d (\bar{\nu}_0 - \Delta\bar{\nu})^4 N \beta (\bar{\nu}_{ref} - \Delta\bar{\nu})^{-4} \quad (2)$$

Several practical studies have examined the effect of particle size on Raman response in crystalline powders or grains,<sup>[29–33]</sup> and some of these articles<sup>[30,32]</sup> show that smaller particles can lead to an increase of intensity, which is contrary to the findings of Schrader et al.<sup>[28]</sup> Most of these previous studies involve particle sizes greater than 10  $\mu\text{m}$  or particles compacted in pellets to examine the Raman response from pharmaceutical tablets, which is less relevant to the subject of this article.

This study examined aerosol particles scattered onto a thin reflective filter (silver) and focused on health-related particle size fractions and environmental sample fractions of aerosol particulates (0.5 to 10  $\mu\text{m}$ ). These diameters are much closer to the wavelength of the incident energy, that is, an NIR laser of 0.785  $\mu\text{m}$  than particles studied in previous work.

## 2 | METHOD

The experiments were designed in three stages. First, a calibration was developed using the respirable quartz reference material A9950 (Health and Safety Executive [HSE], Buxton, UK). A9950 is a high purity quartz reference material with a crystallinity of 89.3%.<sup>[9]</sup> Second, the measurement response for the XRD and Raman spectroscopy was compared for different size fractions of A9950 collected using a Sioutas impactor,<sup>[34]</sup> and a calibration mass correction factor was determined to correct the measured mass for any reduction in XRD or Raman spectroscopy response at small particle diameters. Third, XRD and Raman spectroscopy measurements of crystalline silica were compared for samples of dust generated from the cutting and polishing of natural and artificial stones.

## 2.1 | Calibration of XRD and Raman spectroscopy instruments

Raman measurements were collected using an In-Via microscope (Renishaw Ltd, Gloucester, UK) with an NIR (785 nm) laser with a line output at 300 mW, and 110 mW on the sample, without attenuation. XRD measurements were obtained using an X-pert Pro MPD instrument (PANalytical Ltd, Cambridge, UK) with focusing Bragg–Brentano geometry and X-pert for Industry software (Malvern Panalytical Ltd, Malvern, UK).

XRD and Raman spectrometry measurement conditions and methods to determine the limits of detection (LODs) are described in previous articles<sup>[21,35]</sup> and in the Supporting Information.

Calibration samples for XRD and Raman spectroscopy were prepared by filtering aliquots (0.25 to 9 ml) from a 201  $\mu\text{g ml}^{-1}$  suspension of A9950 in isopropanol into a 15-mm-diameter area on 0.45- $\mu\text{m}$ -pore-size silver filters (SKC Ltd, Blandford Forum, Dorset, UK). A suspension of 14.7  $\mu\text{g ml}^{-1}$  was used for lower loadings. The area of the sample deposit was constrained to 176.7  $\text{mm}^2$  using a bespoke 15-mm-diameter filtration funnel. The preparation of calibration samples to aid a uniform deposit is described in previous articles.<sup>[21,24]</sup> The mass of sample loaded onto the silver filters was kept below 1000  $\mu\text{g}$  to avoid correcting for sample absorption when using XRD.<sup>[36]</sup> The calibration response trend line was extended up to 1800  $\mu\text{g}$  to examine the effect of the depth of sample on Raman band intensity.

## 2.2 | Generation of samples of A9950 to assess stability of the Raman band response

A Sioutas impactor aerosol sampler<sup>[34]</sup> was used to collect aerosols of A9950 generated in a containment box within a fume cupboard. This impactor aerosol sampler selects particles following the particle selection criteria defined for environmental health-related monitoring. The Sioutas separates the captured aerosol into four fractions for particles between 10 and 2.5  $\mu\text{m}$ , 2.5 and 1  $\mu\text{m}$ , 1 and 0.5  $\mu\text{m}$  and 0.5 and 0.25  $\mu\text{m}$ . PM10 is the sum of all the fractions, whereas PM2.5 is the sum of the three fractions excluding the 10 to 2.5- $\mu\text{m}$  cut. Particles less than 0.25  $\mu\text{m}$  are captured on an exit filter.

The Sioutas impactor was calibrated to operate at its specified flow rate of 9  $\text{L min}^{-1}$  using a TSI 4100 flow metre (TSI Inc, USA). Size fractions of A9950 were collected on 0.5- $\mu\text{m}$ -pore-size polytetrafluoroethylene (PTFE) filters (SKC UK Ltd, Blandford Forum, UK)

placed on each impactation stage. Dust collected onto PTFE filters was washed into glass bottles with isopropanol and filtered into a 15-mm-diameter area on 0.45- $\mu\text{m}$ -pore-size silver filters for analysis. An amount of isopropanol was placed into a borosilicate glass bottle, which was sufficient to cover a PTFE filter. PTFE filters containing sample were inserted into the glass bottle and wetted with the isopropanol. The filter was then held with tweezers close to the surface of the isopropanol, and the remaining dust was washed or scrapped into the liquor with a spatula. The filter, spatula and sides of the glass bottle were washed with isopropanol into the liquor. The suspension was then filtered onto silver filters following the previously described procedure.

The proportions of A9950 were then measured on each silver filter using XRD and Raman spectroscopy.

Twelve filters (three from each impactor stage) were used to assess the potential for loss of dust during the recovery and filtration processes. The weight of dust collected on the PTFE and silver filters was determined gravimetrically using a balance with a readability of six decimal places (Sartorius UK Ltd, Epsom, UK). The average recovery and its standard deviation were recorded for the 12 filters.

The XRD and Raman spectroscopy responses were also compared when measuring the respirable fraction of aerosolised quartz standard Quin B collected using the GK 2.69 respirable sampler (Mesa Labs, Lakewood, Colorado, USA) operating at a flow rate of 4.2  $\text{L min}^{-1}$ . The GK 2.69 sampler was used with an adaptor for a 25-mm-diameter PVC filter in a conductive filter cassette. The PVC filters collected from the respirable sampler were placed into glass bottles and ashed using a low-temperature plasma asher (Emitech K1050X, Quorum Technologies Ltd, Ashford, UK). The filters were ashed in air at 50% power for 12 h and then in oxygen for 4 h at 95% power. About 5 ml of isopropanol was added to the bottle after it was removed from the asher. The liquor and residue were then sonicated for about 2 min and filtered into a 15-mm-diameter circular area on 0.45- $\mu\text{m}$ -pore-size silver filters.

Bulk samples of A9950 and Quin B quartz reference materials were used to evaluate the measurement response for quartz dusts with median particle sizes from about 4 up to 7  $\mu\text{m}$ . The quartz reference material Quin B (Institut National de Recherche et de Sécurité [INRS], France) has a crystallinity of 95.5% and a median particle size closest to the thoracic fraction (median diameter of 7.2  $\mu\text{m}$  when measured using laser diffraction). The quartz reference material A9950 has a median diameter of 4.2  $\mu\text{m}$ .

About 1 mg of bulk quartz powder (A9950 or Quin B) was weighed into a glass bottle, sonicated for 2 min in



isopropanol and filtered into a 15-mm-diameter area on a pre-weighed silver filter. Three replicate samples were prepared for each powder.

A two-sided *t* test was used to compare if the XRD and Raman spectroscopy measurements made on the same samples were similar, for each size fraction, with a 95% level of confidence. A probability (*p*) value greater than 0.05 would indicate that the results for each instrument were not significantly different.

Laser diffraction particle size measurements were used to verify the particle size distribution of the A9950 collected by each particle size fraction. The particle size measurements were conducted by Particle Technology Ltd (Hatton, Derbyshire, UK) using a Horiba LA950 laser diffraction particle size analyser (Horiba UK Ltd, Northampton, UK). The laser diffraction instrument reports the volume distribution of sphere diameters.

The mass of the quartz particle and the mass of the crystalline quartz are different when particles are small, which may affect the instrument response.<sup>[14,16]</sup> To compare the relationship between Raman response and crystallinity, the relative mass response for each particle size fraction was plotted with a line showing the proportion of crystalline quartz for particles with a disordered layer of 0.03 μm. The predicted crystallinity was calculated by making the assumption that these particles were spherical and by calculating the volume for the particle and the crystalline material, where the radius is reduced by 0.03 μm. The volume crystalline material was then divided by the total volume of the particle for each median particle size value from each size fraction. A volume spherical diameter is similar to that measured by a laser diffraction instrument and equates to an aerodynamic diameter for small particles.

A mass correction factor ( $\bar{X}$ ) for the average difference in response per unit mass from the calibration was calculated for each impactor stage using the ratio:

$$\bar{X} = \frac{1}{n} \sum (M_T/m_I) \quad (3)$$

where  $M_T$  represents the mass of particles collected by an impactor size fraction, determined gravimetrically,  $m_I$  is

the mass reported using the instrument (XRD or Raman spectroscopy) and *n* is the number of ratios. This average ratio was applied to correct for any reduction in instrument response from the calibration at small particle diameters.

### 2.3 | Samples from cutting and polishing of stones

Cutting and polishing tests were conducted on sandstone, two engineered (resin-containing) stones, a natural stone known as diorite (which is an igneous rock related to granite) and a sintered stone. The mineral composition of each of these stones was measured using XRD and the Rietveld method with an internal standard. The generation of emissions from the powered cutting and polishing of stones was carried out in a dust tunnel (Figure 1), which is a long box about 1.5 m high and 1 m wide. The stones were held on a traverse, which moved the stone in the *x* and *y* directions whilst the stone was cut or polished. A fan moved air from outside the building through the dust tunnel past the traverse and towards a rotating manikin, which simulated the presence of a worker and was used as the sampling position. A turbulence grid with three ionising fans was positioned downstream of the emission and used to reduce eddies and improve mixing of the generated aerosols.

A GK 2.69 sampler with a cassette for a 37-mm-diameter PVC filter collected the respirable fraction, whilst another GK2.69 sampler operating at 1.6 L min<sup>-1</sup> collected the thoracic fraction.<sup>[37]</sup> A Sioutas impactor operating at its specified flow rate of 9 L min<sup>-1</sup> was used to collect the environmental particle size fractions within PM10. The GK 2.69 samplers were placed on the front of the rotating manikin on the chest, and the Sioutas sampler was placed on its back at about the same height. Three replicate tests were performed with the GK 2.69 samplers and two with the Sioutas impactor. The filter samples from the respirable and thoracic samplers were ashed following the procedure previously described. The Raman band response for each impactor stage for each dust was compared with the response obtained from

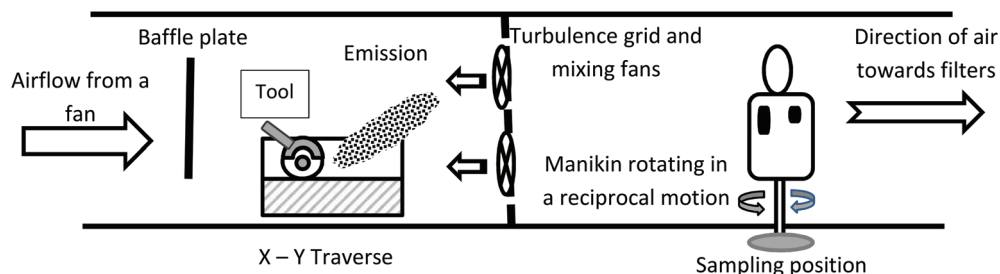


**FIGURE 1** Configuration of the dust tunnel, not to scale [Colour figure can be viewed at [wileyonlinelibrary.com](http://wileyonlinelibrary.com)]

XRD (which is related to the crystallinity of the quartz particulate). In addition, the mass of quartz particulate collected in each impactor stage was estimated by applying the mass correction factor ( $\bar{X}$ ) to the measured Raman band and XRD responses.

### 3 | RESULTS

The mass response trend lines achieved for Raman spectroscopy when pipetting aliquots of A9950 onto silver filters are shown in Figure 2. The stability of the average area responses from typical particle loadings from each stage from a Sioutas impactor is shown in Figure S3. Scanning electron microscope (SEM) images of the density of particles at various mass loadings are shown in Figure S4. Particles appeared to be a continuous layer from a loading of about 500  $\mu\text{g}$  and are stacked on top of each other in the image at 1000  $\mu\text{g}$ . The trend lines for XRD are shown in Figure S5. The maximum mass value for the XRD calibration was about 1000  $\mu\text{g}$  because of the significant absorption of the X-ray response (about 20%) at higher mass loadings<sup>[36]</sup> when quartz is deposited on a 15-mm-diameter area. The LODs from the two

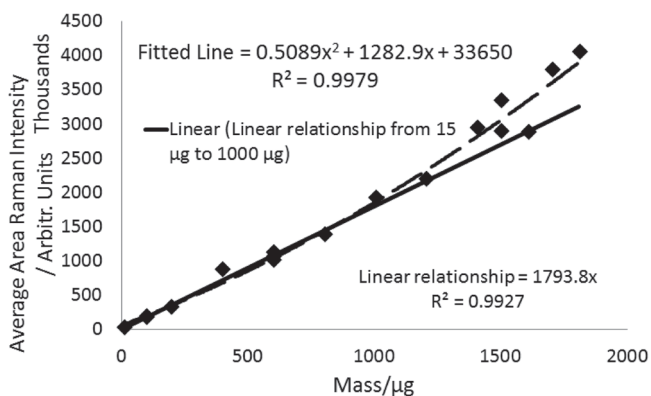


FIGURE 2 Relationship between Raman responses for a mass of quartz loaded into a 15-mm-diameter area onto a silver filter

#### XRD

Angle of reflection ( $2\theta$ )	20.9	26.6	50.1
Measurement of blank filters	11 $\mu\text{g}$	1 $\mu\text{g}$	13 $\mu\text{g}$
By calculation. From the variability of the background scatter	14 $\mu\text{g}$	3 $\mu\text{g}$	21 $\mu\text{g}$

#### Raman

Measurement of blank filters	0.210 $\mu\text{g}$
By calculation. From the variability of the background scatter	0.085 $\mu\text{g}$

Abbreviation: XRD, X-ray diffraction.

approaches for the Raman spectroscopy and XRD measurements are listed in Table 1.

The average recovery of fractions of A9950 from 12 PTFE Sioutas impactor filters and onto the silver filters was  $100 \pm 3.8\%$  ( $1\sigma$ ). The mass loadings ranged from 890 to 1300  $\mu\text{g}$  for the 2.5- to 10- $\mu\text{m}$  impactor stage and from 102 to 120  $\mu\text{g}$  for the 0.25- to 0.5- $\mu\text{m}$  stage. The particle sizes of A9950 collected by each impactor filter and the bulk quartz reference dusts were measured using laser diffraction. They are also shown in Table 2 with the average percentage mass response from each technique, the standard deviation of the replicate analyses and the  $t$ -test probability value for each set of techniques.

Figure 3 shows the change in instrument response per unit mass for each measured particle size fraction. A curve for the predicted crystallinity of quartz particles for various diameters with a disordered surface layer of 0.03  $\mu\text{m}$ <sup>[10]</sup> is also shown. The average Raman spectroscopy values are significantly higher than those from XRD for the two impactor stages covering the smallest particles (1 to 0.5  $\mu\text{m}$  and 0.5 to 0.25  $\mu\text{m}$ ). The  $p$  values from the  $t$  tests are 0.13, 0.02, <0.01 and <0.01 for the 10- to 2.5- $\mu\text{m}$ , 2.5- to 1- $\mu\text{m}$ , 1- to 0.5- $\mu\text{m}$  and 0.5- to 0.25- $\mu\text{m}$  impactor stages, respectively (Table 2). The XRD results obtained in this research are comparable with those obtained by Page,<sup>[12]</sup> who measured samples of a grade of quartz dust known as Min-U-Sil 10 (Figure S6).

### 3.1 | Stone cutting and polishing tests

Paired XRD and Raman spectroscopy results were obtained from a total of 119 emission test samples, which included 72 impactor and 47 respirable and thoracic samples. In total, there were 24 XRD values below the lowest estimated LOD of 1  $\mu\text{g}$  and four Raman spectroscopy values below the highest estimated LOD of 0.21  $\mu\text{g}$ . The mass percentages of crystalline silica and other crystalline mineral components in the sandstone and engineered (resin-containing), diorite and sintered stones used in the

TABLE 1 Limits of detection

(LODs) for the XRD and Raman spectroscopy methods when measuring quartz on clean blank filters, ashed and deposited in a 15-mm-diameter area on a silver filter, and when calculating the LOD for quartz from the variability in the background scatter

**TABLE 2** Particle size statistics measured by laser diffraction for fractions of aerosolised quartz reference material A9950, and the bulk powders of A9950 and Quin B, the average percentage of quartz measured with standard deviation and the *t*-test probability that the XRD and Raman reported values for the per cent crystallinity

Particle size range	Mean diameter (μm)	Median diameter (μm)	Technique	Number of samples (n)	Average per cent crystallinity and standard deviation (1 σ)	<i>t</i> -test probability (p)
Impactor Stage 4 0.25 to 0.5 μm	0.6	0.54	XRD	4	27.6 ± 8.0	<0.01
			Raman	4	54.9 ± 7.7	
Impactor Stage 3 0.5 to 1 μm	0.88	0.85	XRD	4	72.4 ± 4.5	<0.01
			Raman	4	83.5 ± 2.4	
Impactor Stage 2 1 to 2.5 μm	1.34	1.31	XRD	4	89.8 ± 5.0	0.02
			Raman	3	101 ± 3.0	
Impactor Stage 1 2.5 to 10 μm	3.43	2.93	XRD	4	105 ± 4.7	0.13
			Raman	3	99.2 ± 3.0	
Quin B (respirable fraction)	3.03	2.59	XRD	3	99.9 ± 0.7	0.97
			Raman	3	99.9 ± 2.1	
A9950	4.85	4.20	XRD	3	107 ± 2.0	0.01
			Raman	3	100 ± 1.8	
Quin B	7.20	7.20	XRD	3	112 ± 0.2	<0.01
			Raman	3	92.2 ± 4.2	

Abbreviation: XRD, X-ray diffraction.

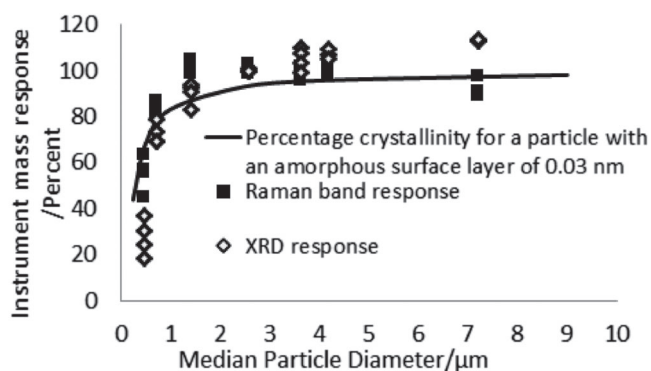


**FIGURE 3** Relative Raman spectroscopy and X-ray diffraction (XRD) responses when measuring size fractions of the quartz reference material A9950

emission tests are shown in Table 3. Results comparing the instrument response and estimated mass of crystalline silica measured by XRD and Raman spectroscopy in each Sioutas particle size fraction for the samples collected from the cutting and polishing of engineered stone and sandstone are shown in Figure 4 for power cutting and Figure 5 for polishing. Results for diorite and sintered stones are in Figure S7 (cutting) and Figure S8 (polishing). The results for XRD are shown in the charts on the left-hand side, and the Raman spectroscopy measures, reported on the same samples, are shown in the

charts on the right-hand side. The solid lines in the charts in these figures represent the instrument response. The broken lines on these charts represent the calculated values for the mass of quartz particles when the mass correction factor was applied. The XRD mass response correction factors were 0.95, 1.11, 1.38 and 3.62, and the Raman spectroscopy mass response correction factors were 1.00, 0.98, 1.20 and 1.82 for the 10- to 2.5-μm, 2.5- to 1-μm, 1- to 0.5-μm and 0.5- to 0.25-μm impactor stages, respectively.

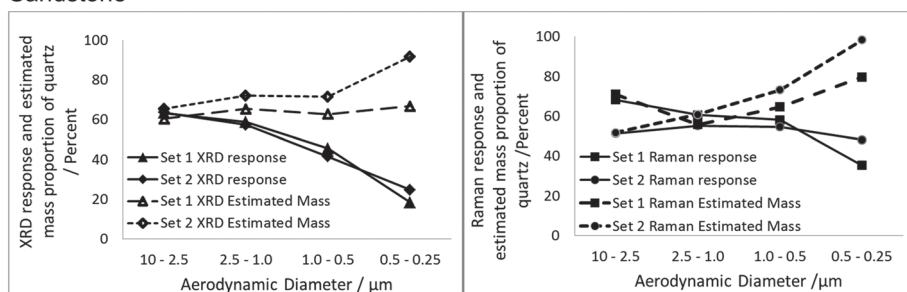
For cutting stone, the range of loadings on the impactor samples was from 1600 to 700 μg for the 10- to 2.5-μm stage down to 122 to 72 μg for the 0.5- to 0.25-μm stage. When polishing, the range of loadings on the impactor filters was from 787 to 330 μg for the 10- to 2.5-μm stage down to 37 to 19 μg for the 0.5- to 0.25-μm stage. For the samples from cutting, two XRD values were less than the LOD (1 μg) for the smallest size fraction; for the sintered stone and diorite samples (and hence the missing data points in Figure S7), only one Raman spectroscopy measurement reported an LOD when measuring the same samples. For the samples collected from polishing, 14 XRD values were below the LOD. In contrast, Raman spectroscopy was not able to report two results from the polishing activity. The two Raman spectroscopy measurements were on samples collected from the sintered stone (Figure S8). One Raman spectroscopy measurement was



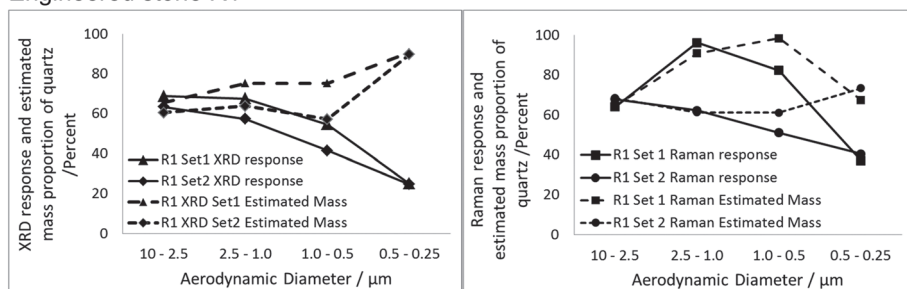
Material	Mass per cent crystalline silica (quartz) SiO <sub>2</sub>	Other mineral phases Per cent crystalline content
Sandstone	62	Albite (NaSi <sub>3</sub> O <sub>8</sub> ) 7.5% Kaolinite (Al <sub>2</sub> Si <sub>2</sub> O <sub>5</sub> (OH) <sub>4</sub> ) 2.2%
Engineered stone R1	67	Albite (NaSi <sub>3</sub> O <sub>8</sub> ) 14%
Engineered stone R2	89	Rutile (TiO <sub>2</sub> ) 2.2%
Diorite	7.2	Anorthite (CaAl <sub>2</sub> Si <sub>2</sub> O <sub>8</sub> ) 51% Diopside (MgCaSi <sub>2</sub> O <sub>6</sub> ) 35% Mica (KAl <sub>2</sub> (AlSi <sub>3</sub> O <sub>10</sub> )(OH) <sub>2</sub> ) 2.4% Hornblende ((Ca,Na) <sub>2</sub> (Mg,Fe,Al) <sub>5</sub> (Al, Si) <sub>8</sub> O <sub>22</sub> (OH) <sub>2</sub> ) 3.4%
Sintered stone S1	6.9	Zircon (ZrSiO <sub>4</sub> ) 16% Mullite (3Al <sub>2</sub> O <sub>3</sub> 2SiO <sub>2</sub> ) 12%

TABLE 3 Composition of crystalline minerals in the stone samples

### Sandstone



### Engineered stone R1



### Engineered stone R2

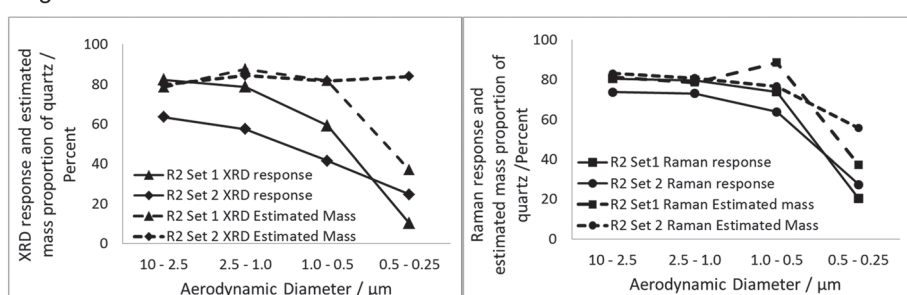


FIGURE 4 Cutting of artificial and natural stones. Relative instrument response and estimated mass proportions of quartz obtained by X-ray diffraction (XRD) and Raman spectroscopy when measuring size fractions collected by the Sioutas impactor sampler

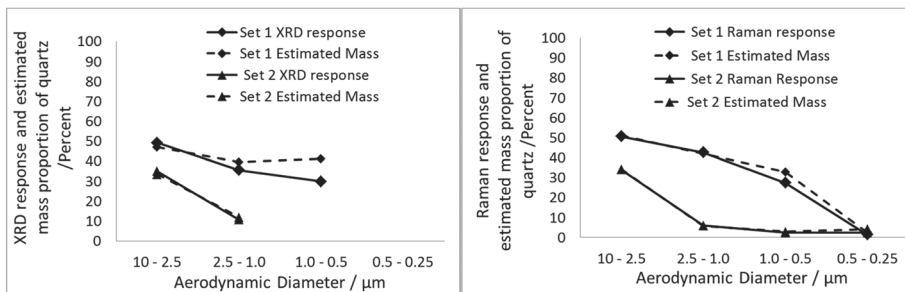
below the LOD, and the other had too much fluorescence in each spectrum. The sample with too much fluorescence was from the impactor filter collecting the 10- to

2.5-µm particle size fraction and had more than 1 mg of dust. The highest loaded impactor samples (around 1 mg) were affected by excessive occurrence of detector

saturation. A subsample, with less loading, was obtained for some samples by suspending the dust from the filter in isopropanol, taking an aliquot of the suspension and filtering this suspension to produce a sample with a lower particle density than was previously measured. Figures 6–8 compare the correlations between mass values for crystalline silica obtained by XRD and Raman spectroscopy when measuring the impactor (Figure 6), respirable (Figure 7) and thoracic samples (Figure 8), during the cutting and polishing of the stones. Both the x and y axes are log<sub>10</sub> scale. The dotted lines on the charts in Figures 6–8 represent the ideal 1:1 relationship. The

paired XRD and Raman spectroscopy results from the impactor samples were corrected for changes in response due to particle size by multiplying the measured value with the mass correction factor for its size fraction. The coefficient for the slope of 0.97 for the impactor samples was not significantly different from the ideal relationship 1.00 (95% confidence level for the range of slope values was 0.94 to 1.00). Eight XRD values, for the respirable and thoracic dust samples from polishing, were not reported because they were less than the LOD of 1 μg, whereas only three values were not reported when measured using Raman spectroscopy (LOD of 0.21 μg).

Sandstone



Engineered stone R1

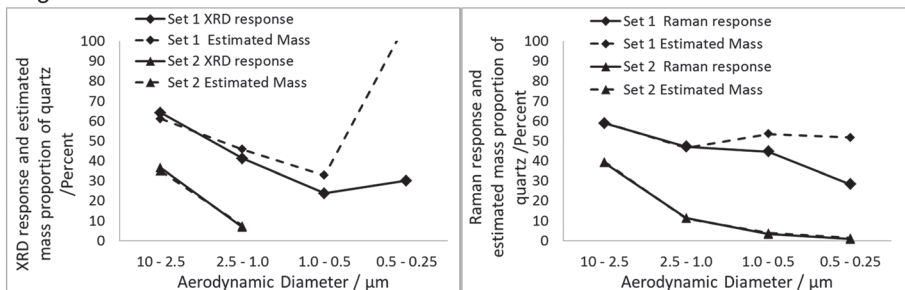


FIGURE 5 Polishing of artificial and natural stones. Relative instrument response and estimated mass proportions of quartz obtained by X-ray diffraction (XRD) and Raman spectroscopy

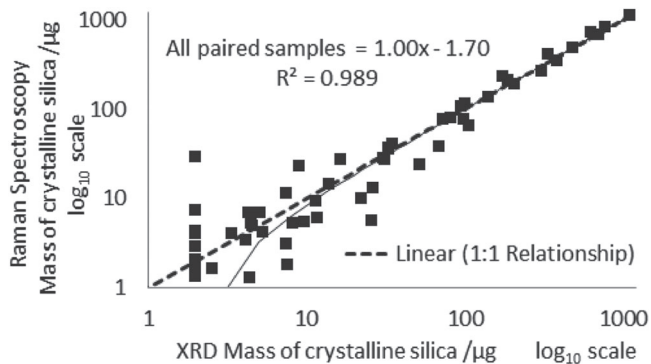


FIGURE 6 A comparison of Raman and X-ray diffraction (XRD) measurements of crystalline silica in the fractions of aerosol collected by the Sioutas impactor for all samples (from cutting and polishing). The results are corrected for the change in measurement XRD and Raman response for small diameter particles (less than 1 μm in diameter) due to the reduction in crystallinity

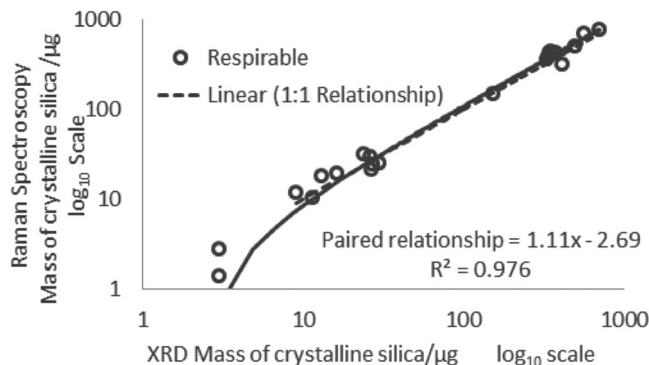
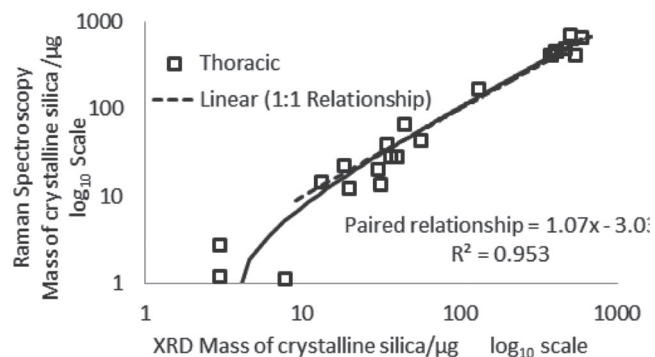


FIGURE 7 The respirable fraction. A comparison of Raman and X-ray diffraction (XRD) measurements of crystalline silica collected from cutting and polishing of sandstone, engineered stone, diorite stone and sintered stone



**FIGURE 8** The thoracic fraction. A comparison of Raman and X-ray diffraction (XRD) measurements of crystalline silica collected from cutting and polishing of sandstone, engineered stone, diorite stone and sintered stone

Coefficients of determination for the paired relationships were 0.97 and 0.95 with slope values of 1.11 and 1.06 for the respirable and thoracic samples, respectively. The slope value for the RCS analyses was significantly different from the ideal value of 1.00 at the 95% level of confidence (the range of values within a 95% level of confidence was 1.03 to 1.19) but not for the thoracic samples (the range of slope values within a 95% level of confidence was 0.96 to 1.17).

## 4 | DISCUSSION

### 4.1 | The use of Raman spectroscopy for exposure measurement

Raman spectroscopy has a clear benefit over XRD in terms of its ability to measure samples with lower masses of quartz and its sensitivity when measuring particle sizes less than 1  $\mu\text{m}$  (Figure 3). Its LOD is between 0.085 and 0.210  $\mu\text{g}$ , which is 14 times lower than that calculated for the most sensitive XRD reflection. The benefit of applying a Raman spectroscopy method based on the averaged accumulated spectra from multiple micro-area measurements is that the occasional spectra with fluorescence or detector saturation can be ignored, because the average value is fairly consistent (Figure S3), so long as sufficient measurements are recorded. Nearly every sample had an occasional spectrum where saturation of the detector occurred, which was discounted for the calculation of the average value. Excess fluorescence prevented the measurement of just one single sample in the 119 that were measured in these tests. This particular sample of zircon had a high mass loading (greater than 1 mg) in the 10- to 2.5- $\mu\text{m}$  fraction. Loadings greater than 1 mg are not frequently encountered for

occupational hygiene sampling of RCS. The low incidence of measurement failure on these challenging samples and good correlation of Raman spectroscopy and XRD measurements (Figures 6–8) demonstrates the robustness of the Raman spectroscopy method for samples from stone working activities. The results from the impactor samples (Figures 4 and 5) show that, in general, Raman will give results for samples containing crystalline silica that are similar to those measured by XRD. Most paired XRD and Raman spectroscopy results are close to the ideal relationship of 1.00 (Figure 7), despite some additional variability from the lowest impactor stage samples. The calculated mass proportions of quartz particulate are similar for each particle size fraction from cutting and polishing, although the values from cutting are closer to the proportion of crystalline silica in the bulk material than for polishing. The variability in the estimated mass values obtained for the impactor stage with the lowest particle size fraction could be due to (a) measurement errors for low masses of crystalline silica in the presence of significant mineral interference (e.g., for the diorite samples with only 7% quartz in an anorthite matrix) and (b) correction errors caused by some migration of particles from the third to the fourth impactor stage. Particle bounce from one stage to another is a phenomenon that can occur when the impaction collection mediums are heavily loaded.<sup>[38]</sup>

Spectra and scans showed that Raman spectroscopy is of greater benefit than XRD when measuring samples containing zircon ( $\text{ZrSiO}_4$ ). Zircon is fully resolved when using Raman spectroscopy (Figure S9) and potentially more accurately measured, whereas it is a significant interference for the main quartz reflection at 26.6° when using XRD (Figure S10). There is also interference of the Raman band shift for quartz at 464  $\text{cm}^{-1}$  from some common feldspar mineral components like albite, anorthite and microcline; however, these were resolved using the peak fitting software in the Raman spectroscopy instruments WIRE™ operating program (Figure S11). The mapping process also allows for occasional Raman spectrum with too much interference to be omitted, because the mean density of particles over the filter surface should be reasonably consistent. XRD has similar issues with interference from silicate minerals<sup>[39]</sup> (Figure S12).

A significant issue for Raman spectroscopy is the presence of rutile (titanium oxide,  $\text{TiO}_2$ ). Rutile was found as a contaminant in the engineered stone samples (about 0.5% to 2%), although it is not usually present in other workplace samples for RCS measurement. Rutile bands were difficult to resolve from quartz and may have contributed to some high Raman spectroscopy values

(+10% to +20%) when compared with XRD results. Despite these potential issues, the slope coefficient between Raman spectroscopy and XRD measurements for crystalline silica, from cutting and polishing stone, is close to the ideal of 1.00. One disadvantage for practical work is that Raman spectroscopy is not able to cope with excess filter residue as well as XRD. Occasional incidents of visible excess filter residue were thought to be the cause for the single points significantly below the trend line for the 1:1 relationship in Figures 7 and 8. However, excess filter residue after ashing is probably not significant when dealing with more routine samples in the United Kingdom. The GK 2.69 samplers used 37-mm-diameter filters in anticipation of some high loadings of aerosol, whereas most respirable samplers in the United Kingdom use 25-mm-diameter filters that substantially reduce the amount of material (by about 55%).

A high background level in the Raman spectrum was a significant issue for the first set of samples of engineered stone (R1) prepared for measurement, which was attributed the use of an old set of silver filters with a rougher scratched surface. The measurement time had to be reduced to permit analysis, which resulted in broader Raman bands and curved backgrounds, which makes the fitting of the band profile difficult when using the software and a linear background correction.

## 4.2 | Response due to particle size and sample depth

The calibration encompassed samples with a range of particle densities from scattered particles in each field of view to multilayers (Figure S4).

Figure 2 indicates that the Raman band intensity is proportionally related to the volume of particles ( $N$ ) within the cross-sectional area of the laser ( $A$ ) (Equation 2) when the loading is below 1000  $\mu\text{g}$ .

At low particle densities, the depth of the sample ( $d$ ) is effectively the particle diameter and the absorption ( $\alpha$ ) is from the particle itself, because other particles are not close enough to influence the Raman scattering. Therefore, the scattering coefficient ( $s$ ) will depend on the volume of particles within the illuminated cross-sectional area. The character of the Raman band intensity changes at higher mass loadings from one where there are relatively small variations in depth to one where more particles are packed in multilayers within the volume of the focused laser. Factors like absorption and multiple scattering, of laser, Rayleigh and emitted Raman photons (Equation 1) by adjacent particles, are more prevalent and will contribute to the Raman scattering collected by the optics. The increase in Raman scattering coincides

with significant attenuation for XRD measurements, which (for calibration samples) is attributed with point at which sufficient multilayers of particles are present to prevent XRD radiation from fully penetrating into the sample.<sup>[36]</sup> Figure 2 also shows that the intensity has not achieved its maximum penetration depth, because it has not yet reached a plateau.<sup>[28]</sup>

The relative response for the Raman band at 464  $\text{cm}^{-1}$  is fairly constant for particles with diameters from about 1 to 7  $\mu\text{m}$  (Figure 3) and closely follows the predicted proportion of crystalline material for particles with an amorphous/disordered structural surface layer of 0.03- $\mu\text{m}$  depth, as described by Foster and Walker<sup>[10]</sup> and Nagelschmidt et al.<sup>[14]</sup> This demonstrates the relationship between the Raman area band response and the crystallinity of the particle. This finding is expected because the area intensity for both XRD and Raman spectroscopy<sup>[40]</sup> is closely related to the molecular symmetry in the crystal structure.

For example, the principal Raman shift at 464  $\text{cm}^{-1}$  is related to the oxygen (O) motion in the plane of Si–O–Si atoms of silicon (Si) and oxygen.<sup>[41]</sup> Sato and McMillan<sup>[41]</sup> demonstrated that it is the oxygen atoms that contribute most to the intense Raman band shift for quartz at 464  $\text{cm}^{-1}$ , whereas the silicon atoms remain relatively stationary within their structural arrangement. Raman spectroscopy was significantly more sensitive when measuring particle size fractions below 1  $\mu\text{m}$ . It is possible that the Si–O–Si plane of molecular symmetry extends further into the surface layer of quartz and that some Raman scattering will still be emitted from Brillouin zones within the more disordered structure.<sup>[40]</sup>

Most practical studies<sup>[30,32,33,42,43]</sup> show an increase in Raman band intensity with decreasing particle size. However, Chio et al.<sup>[31]</sup> found that the response increased with particle size when studying grains of quartz. Moreover, Hu et al.<sup>[42]</sup> demonstrated a curved relationship for one crystalline polymorph where the Raman band response increases as particle size decreases and reaches a plateau before decreasing with decreasing particle size for the smallest particles. Hu et al.<sup>[42]</sup> and Chio et al.<sup>[31]</sup> studied relatively large particle sizes (64- to 215- $\mu\text{m}$  and 11- to 250- $\mu\text{m}$  grain size, respectively), and both proposed that the analysis volume was a major influence affecting the measurement response and particle size; that is, particle size effects were reduced for larger particle sizes by increasing the laser sampling volume. This hypothesis is supported by the Monte Carlo simulations of Raman scattering in solids and powders studied by Duy et al.<sup>[44]</sup> Duy et al.<sup>[44]</sup> examined pellets and powders of pure lactose with different particle sizes (38 to 382  $\mu\text{m}$  in diameter) using three different instrumental arrangements. Modelling the scattering of photons showed that



the scattering centre moves deeper into the particle and has a broader direction of scatter as the particle size increases. Duy et al.<sup>[44]</sup> found that, in practice, the relationship between response and particle size was dependent on the geometric etendue of the instrument. The number of photons counted could increase with particle size when the detector area was much larger than the illumination area ( $\times 4.2$ ) but could also decrease when the two areas were more similar ( $\times 1.6$ ) because the laterally scattered photons on larger particles were not detected as efficiently. Previous method development work showed a decrease in measurement sensitivity when using the quartz reference material with the largest particle size (Quin B),<sup>[24]</sup> suggesting that the instrument arrangement proposed for the measurement method was not efficiently collecting the laterally scattered photons for the very largest particles in this instance. In this research, reported herein, the minimum area of the focused spot was  $4.5 \mu\text{m}^2$ , which is slightly less than the median diameter of the particles of Quin B ( $7 \mu\text{m}$ ). Moving to a lower magnification objective to increase the collection of laterally scattered photons will not improve the intensity of the Raman scatter, because the lower magnification with low numerical aperture has a smaller angle of light collection.<sup>[45]</sup>

Fine grains studied in this work are smaller than those previously investigated and will scatter photons in a relatively localised area close to the particles' surface, which will be efficiently collected by the detector when using the current optics applied by the method proposed by Stacey et al.<sup>[24]</sup>; that is, the proportion of laterally dispersed photons is small for particles in this study. These conditions may account for the plateau for Raman band intensity observed in this research, for fractions of quartz particles with median diameters between 1 and  $7 \mu\text{m}$ .

## 5 | CONCLUSION

Raman spectroscopy is a promising alternative to XRD for measurement of RCS and has a much lower LOD of around  $0.2 \mu\text{g}$ . The technique is highly correlated with XRD, when measuring the respirable and thoracic health-related particle size fractions of aerosols, generated from the cutting and polishing of natural and artificial stones, and demonstrates the useful application of Raman spectroscopy when analysing workplace exposure samples from stonemasonry activities. In particular, Raman spectroscopy has a distinct advantage over XRD when measuring crystalline silica in samples containing significant levels of zircon (about 50%).

The Raman band response for crystalline silica increases with mass loading of aerosols when using a

standard sized deposition area. The point at which the Raman band response increases, more than the slope for a linear relationship, coincides with the mass at which the XRD response attenuates as a result of X-ray absorption, that is, matrix absorption due to multiple layers. In effect, the XRD results would under-predict when the Raman spectroscopy measurements start to over-predict the 'true' value. This suggests that there was a relationship between X-ray absorption and scattering of Raman photons when the measurement conditions used in this study were applied.

The Raman band response is closely related to the predicted crystallinity of the quartz particle. A slight drop in intensity at  $7 \mu\text{m}$  is probably due to the geometric etendue of the instrument.

## ACKNOWLEDGEMENTS

Thanks to Ian Pengelly, Laurie Davies, Margaret Wade and Susan Hambling who reviewed the article, to Matthew Jackson and Alwyn Sowerby for the gravimetric, Jack Mellor who did some XRD analysis on the bulk materials and Lidia Malecka who helped graphically redraw some spectra (all Health and Safety Executive).

## DISCLAIMER

The opinions expressed in this article are those of the authors alone and do not necessarily represent the policy or views of the Health and Safety Executive.

## ORCID

Peter Stacey  <https://orcid.org/0000-0002-2689-2890>

## REFERENCES

- [1] HSE, *EH75 Respirable Crystalline Silica, Variability in Fibrogenic Potency and Exposure-Response Relationships for Silicosis*, Health and Safety Executive, Richmond, Surrey, United Kingdom **2003**. Report No. ISBN:9780717621910.
- [2] L. Rushton, S. J. Hutchings, L. Fortunato, C. Young, G. S. Evans, T. Brown, R. Bevan, R. Slack, P. Holmes, S. Bagga, J. W. Cherrie, M. van Tongeren, *Br. J. Cancer* **2012**, *107*(Suppl 1), S3.
- [3] T. Brown, J. W. Cherrie, M. Van Tongeren, L. Fortunato, S. Hutchings, *L. R. The Burden of Occupational Cancer in Great Britain Lung Cancer*, Health and Safety Executive, Bootle, Liverpool **2012**.
- [4] NIOSH, *Health Effects of Occupational Exposure to Respirable Crystalline Silica*, Publications Dissemination, 4676 Columbia Parkway, Cincinnati, OH 45226-1998, Department of Health and Human Services, Centers for Disease Control and Prevention, National Institute for Occupational Safety and Health, United States **2002** Contract No.: Publication No. 2002-129.
- [5] CEN, *EN 481:1993 Workplace Atmospheres—Size Fraction Definitions for Measurement of Airborne Particles*, European Committee for Standardisation, Brussels **1993**.
- [6] M. B. Ranade, M. C. Woods, F. L. Chen, L. J. Purdue, K. A. Rehme, *Aerosol Sci. Technol.* **1990**, *13*(1), 54.



- [7] B. Brunekreef, S. T. Holgate, *The Lancet* **2002**, 360(9341), 1233.
- [8] HSE, *Methods for the Determination of Hazardous Substances, MDHS 101/2 Crystalline Silica in Respirable Airborne Dust, Direct On-Filter Analyses by Infrared Spectroscopy and X-Ray Diffraction*, Health and Safety Executive (HSE), Norwich, United Kingdom: Crown **2014**.
- [9] P. Stacey, E. Kauffer, J.-C. Moulut, C. Dion, M. Beauparlant, P. Fernandez, R. Key-Schwartz, B. Friede, D. Wake, *Ann. Occup. Hyg.* **2009**, 53(6), 639.
- [10] R. D. Foster, R. F. Walker, *Analyst* **1984**, 109(9), 1117.
- [11] J. Dodgson, W. Whitaker, *Ann. Occup. Hyg.* **1973**, 16(4), 373.
- [12] S. J. Page, *AIHA Journal*. **2003**, 64(1), 30.
- [13] R. L. Gordon, G. W. Harris, *Nature* **1955**, 175(4469), 1135.
- [14] G. Nagelschmidt, R. L. Gordon, O. G. Griffin, *Nature* **1952**, 169(4300), 539.
- [15] E. J. King, *Occup. Med.* **1947**, 4(1), 26.
- [16] P. B. Dempster, P. D. Ritchie, *Nature* **1952**, 169(4300), 538.
- [17] D. V. Petrov, *J. Optic A: Pure Appl. Optics* **2007**, 9(8), S139.
- [18] G. Schweiger, *J. Aerosol Sci.* **1990**, 21(4), 483.
- [19] D. C. Doughty, S. C. Hill, *J. Quant. Spectrosc. Radiat. Transfer* **2017**, 188, 103.
- [20] P. Vargas Jentzsch, B. Kampe, V. Ciobotă, P. Rösch, J. Popp, *Spectrochim. Acta, Part a* **2013**, 115, 697.
- [21] P. Stacey, K. T. Mader, C. Sammon, *J. Raman Spectrosc.* **2017**, 48(5), 720.
- [22] L. Zheng, P. Kulkarni, M. E. Birch, K. Ashley, S. Wei, *Anal. Chem.* **2018**, 90, 6229.
- [23] J. A. Lynch, Q. T. Birch, T. H. Ridgway, M. E. Birch, *Ann. Work Expo. Health.* **2018**, 62(5), 604.
- [24] P. Stacey, F. Clegg, J. Morton, C. Sammon, *Anal. Methods* **2020**, 12, 2757.
- [25] G. Gouadec, P. Colomban, *Prog. Cryst. Growth Charact. Mater.* **2007**, 53(1), 1.
- [26] S. Osswald, V. N. Mochalin, M. Havel, G. Yushin, Y. Gogotsi, *Phys. Rev. B* **2009**, 80(7), 075419.
- [27] B. Schrader, G. Bergmann, *Fresenius Zeitschrift Anal. Chem.* **1967**, 225(2), 230.
- [28] B. Schrader, A. Hoffmann, S. Keller, *Spectrochim. Acta, Part a* **1991**, 47(9), 1135.
- [29] D. A. Gómez, J. Coello, S. MasPOCH, *Vib. Spectrosc.* **2019**, 100, 48.
- [30] M. V. Pellow-Jarman, P. J. Hendra, R. J. Lehnert, *Vib. Spectrosc.* **1996**, 12(2), 257.
- [31] C. H. Chio, S. K. Sharma, P. G. Lucey, D. W. Muenow, *Appl. Spectrosc.* **2003**, 57(7), 774.
- [32] H. Wang, C. K. Mann, T. J. Vickers, *Appl. Spectrosc.* **2002**, 56(12), 1538.
- [33] P. Kristova, L. J. Hopkinson, K. J. Rutt, *J. Phys. Chem. A.* **2015**, 119(20), 4891.
- [34] C. Misra, M. Singh, S. Shen, C. Sioutas, P. M. Hall, *J. Aerosol Sci.* **2002**, 33(7), 1027.
- [35] P. Stacey, *Powder Diffr.* **2019**, 34(3), 251.
- [36] M. Mecchia, C. Pretorius, P. Stacey, M. Mattenklott, E. Incocciati, X-ray absorption effect in aerosol samples collected on filter media, in *Silica and Associated Respirable Mineral Particles*, (Eds: M. Harper, T. Lee), ASTM International, West Conshohocken, PA, United States of America **2013** 139.
- [37] A. D. Maynard, *J. Aerosol Sci.* **1999**, 30(9), 1227.
- [38] M. Chang, S. Kim, C. Sioutas, *Atmos. Environ.* **1999**, 33(15), 2313.
- [39] ISO B. 16258-1, *Workplace Air—Analysis of Respirable Crystalline Silica Using X-Ray Diffraction. Part 1. Direct-on-Filter Method* (ISO) ISO, editor, British Standards Institution, Chiswick, London **2015**.
- [40] D. Tuschel, *Spectroscopy* **2017**, 32(3), 26.
- [41] R. K. Sato, P. F. McMillan, *J. Phys. Chem.* **1987**, 91(13), 3494.
- [42] Y. Hu, H. Wikström, S. R. Byrn, L. S. Taylor, *Appl. Spectrosc.* **2006**, 60(9), 977.
- [43] A. Sparén, M. Hartman, M. Fransson, J. Johansson, O. Svensson, *Appl. Spectrosc.* **2015**, 69(5), 580.
- [44] P. K. Duy, S. Chun, H. Chung, *Anal. Chem.* **2017**, 89(22), 11937.
- [45] D. Tuschel, *Spectroscopy* **2017**, 32(9), 14.

## SUPPORTING INFORMATION

Additional supporting information may be found online in the Supporting Information section at the end of this article.

**How to cite this article:** Stacey P, Hall S, Stagg S, Clegg F, Sammon C. Raman spectroscopy and X-ray diffraction responses when measuring health-related micrometre and nanometre particle size fractions of crystalline quartz and the measurement of quartz in dust samples from the cutting and polishing of natural and artificial stones. *J Raman Spectrosc.* 2021;1–13. <https://doi.org/10.1002/jrs.6110>